


Crack-healing, a Novel Approach for a Laser-based Powder Bed Fusion of High-performance Ceramic Oxides

Journal Article**Author(s):**

[Verga, Fabrizio](#) ; Makowska, Małgorzata; Cellerai, Guglielmo; Florio, Kevin; Schmid, Manfred; Wegener, Konrad

Publication date:

2021-12

Permanent link:

<https://doi.org/10.3929/ethz-b-000515483>

Rights / license:

[Creative Commons Attribution 4.0 International](#)

Originally published in:

Additive Manufacturing Letters 1, <https://doi.org/10.1016/j.addlet.2021.100021>



Crack-healing, a novel approach for a laser-based powder bed fusion of high-performance ceramic oxides

Fabrizio Verga^{a,b,*}, Małgorzata Makowska^c, Guglielmo Cellera^a, Kevin Florio^a, Manfred Schmid^b, Konrad Wegener^a

^a Institute of Machine Tools and Manufacturing, ETH Zurich, Leonhardstrasse 21, Zurich 8092, Switzerland

^b Inspire AG, Fürstenlandstrasse 122, St. Gallen 9014, Switzerland

^c Laboratory for Nuclear Materials, Laboratory for Synchrotron Radiation and Femtochemistry, Paul Scherrer Institute, PSI, Villigen 5232, Switzerland

ARTICLE INFO

Keywords:

PBF-LB
Additive manufacturing
Ceramic-ceramic composite
Self-healing
Crack-healing

ABSTRACT

Laser-based powder bed fusion (PBF-LB) of ceramic materials have not been developed sufficiently. The process-induced crack formation is the key challenge of the associated additive manufacturing method, which prevents its successful industrial implementation. Therefore, we have adopted a strategy to accept crack formation as an inherent characteristic of the manufacturing process while enhancing the mechanical properties of the parts by repairing the cracks using a thermal post-processing.

Crack healing was successfully demonstrated in the PBF-LB-manufactured alumina titanium carbide (TiC) composite parts after thermal treatment in the air at 900 °C. Crack healing is achieved through the phase transformation from TiC to TiO₂ in the form of rutile. The built parts exhibited a mechanical strength up to two times higher than values demonstrated in the previous studies on alumina PBF-LB without preheating, achieving an average flexural strength value of 181 MPa and a maximum value of 232 MPa.

1. Introduction

Ceramic materials, such as alumina, have a broad range of applications owing to their excellent mechanical strength, wear resistance, thermal properties, and biocompatibility. Moreover, their standard manufacturing process is time consuming and leads to a limited geometrical complexity and high tool wear.

The application of additive manufacturing (AM) can technologically affect the ceramic industry. The design freedom and subsequent achievable geometrical complexity enabled by AM is considerably higher than that of any other manufacturing technology. Laser-based powder bed fusion (PBF-LB) is an AM technique that has been effective in the production of functional prototypes and small-to-medium size production series of polymers and metals. However, applying the PBF-LB technique on the ceramic materials is still under study. The industrialization of PBF-LB in ceramics is strongly limited owing to the moderate ultimate flexural strength of the manufactured components, which arises from the formation of microcracks induced by the extreme thermal gradient generated during the process in addition to the low thermal shock resistance of ceramics [6]. It was proposed to reduce the thermal gradient by preheating the ceramic powder to a temperature near its melting temperature. By preheating up to 1700 °C and employing a low-melting-temperature

Al₂O₃-ZrO₂ eutectic mixture, it was possible to manufacture crack-free samples [17, 36]. However, the large and uncontrolled melt pool, favored by a high preheating temperature, was the origin of the poor surface finish. While preheating solved the problem associated with the microcracks for several millimeters of the build height, larger cracks induced by the thermal gradient within the solidified material itself could not be avoided [16,35]. Many studies have failed to process fully dense and crack-free ceramic parts [3,10,11,19,27,31]. The large number of cracks induced by the process dramatically lowers the ultimate strength of parts, as demonstrated in Table 1. Aside from the high temperature experiments [17,35], only ceramic-glass composites have yielded flexural strengths higher than 100 MPa ([8,12,18,23,29,30]). Glasses have certain advantageous properties, such as a low melting point, small thermal expansion coefficient, and low elastic modulus [21]. However, the presence of glass itself is a significant disadvantage that limits the ultimate strength of these composites compared to crystalline ceramics [20]. The thermal post-processing was proposed and assessed on PBF-LB of yttria-stabilized zirconia, alumina, and alumina-toughened zirconia [3,19,34]. Nevertheless, the mechanical properties of specimens could not be improved. To introduce an effective post-processing, a PBF part needs to maintain a certain reactivity to cause sintering or crack healing. Failure management study has led to the development of self-healing ceramic

* Corresponding author at: Inspire AG, Fürstenlandstrasse 122, St. Gallen 9014, Switzerland.

E-mail address: verga@inspire.ethz.ch (F. Verga).

Table 1
Mechanical properties of PBF-LB ceramic parts compared to fully dense alumina samples manufactured using the standard (STD) sintering process.

Method	Author	Specimens' flexural strengthMPa	Preheating temperature °C	Post processing	Material
AM	[36]	>500	1600	N/A	Eutectic Al ₂ O ₃ -ZrO ₂
AM	(P. [28])	100	20	N/A	Al ₂ O ₃ -SiO ₂
AM	[23]	110	20	Ceracom forging	Al ₂ O ₃ , B ₂ O ₃ and zinc borosilicate glass
AM	[34]	31	20	Furnace 1300 °C-3 h	Al ₂ O ₃ -ZrO ₂
AM	[11]	25	20	N/A	Fe ₂ O ₃ doped Al ₂ O ₃
AM	[13]	12	20	N/A	Al ₂ O ₃ -LiAl(SiO ₃) ₂
STD	[7]	650-350	-	Sintered	Al ₂ O ₃ 99,7% density

materials [40]. When these ceramic composites are exposed to certain conditions, for instance high temperatures and an oxidizing atmosphere, defects autonomously repaired [14,26]. SiC has been extensively studied as a healing agent for aluminum oxide [1,22,32]. Studies conducted on directed energy deposition (DED) [37] showed that SiC could act as a toughening element within an eutectic Al₂O₃-ZrO₂, which shortens the crack length. However, when SiC was employed as a laser coupling agent in PBF-LB, only a limited amount of SiC was found to be beneficial for the process (≥ 0.5 wt.%), and a higher amount resulted in an unstable melting process [25]. Alumina with dispersed titanium carbide (TiC) particles is an interesting example of self-healing composite, in which TiC acts as a healing agent. This composite was demonstrated to be effective in the strength recovery of cracked and subsequently healed flexural specimens produced using the spark sintering [4,38]. The cracks were produced by indentation, resulting in fissures with a surface length of 100 μm and an estimated crack opening distance in the range of 0.1–0.5 μm . In PBF-LB samples, cracks had few hundred micrometers in surface length and up to 2 μm in opening distance. Furthermore, cracks were dispersed within the entire sample. Because of the stability of TiC at high temperatures, TiC was selected in this work as a crack-healing agent for the alumina matrix.

Although crack-healing materials were primarily developed to repair themselves during service, we explore the possibility of using the self-healing properties of Al₂O₃-TiC to restore the mechanical properties of PBF-LB components after manufacturing.

2. Material and methods

2.1. Powder preparation

For this investigation, alumina powder SLA-45 ($D_{10} = 34 \mu\text{m}$; $D_{50} = 50 \mu\text{m}$; $D_{90} = 62 \mu\text{m}$) with a purity $> 99.8\%$ (Anhui Estone Material Technology) and 10 vol% of TiC powder – TiC STD 250 ($D_{10} = 1.3 \mu\text{m}$; $D_{50} = 4.7 \mu\text{m}$; $D_{90} = 10.6 \mu\text{m}$) (Höganäs) – were employed. The alumina and TiC powders were dispersed in a 20% ethanol suspension and mixed using a magnetic stirring device for 30 min. The Al₂O₃-TiC slurry was left to dry overnight in a large shallow vessel. The dried Al₂O₃-TiC powder was finally sieved with a 120 μm mesh before laser processing. The Hausner ratio $H = \rho_t / \rho_a$, defined as the ratio between the apparent density ρ_a and tap density ρ_t of the powder, is an predictor of the rheological properties [15]. The H value for this powder formulation was 1.3, which is acceptable for PBF [33]. Fig. 1(a) shows a scanning electron microscopy (SEM) image of the powder mixture. The large spheres are Al₂O₃ particles, while the small, rugged particles indicate TiC.

2.2. Part preparation and characterization

To assess the performance of this powder on the PBF-LB process, cubes of 10 mm \times 10 mm \times 10 mm were built on a proprietary machine mounting a 200 W Nd-YAG laser emitting in the 1064 nm regime (redPOWER, SPI Lasers Ltd.) with a spot size diameter of approximately

110 μm . The cubes were manufactured on a brass disk coated with a layer of eutectic Sn-Zn alloy with a thickness of 0.5–1 mm to ease the removal [34]. The process was carried out under a N₂ protective atmosphere to prevent premature oxidation of the TiC particles, O₂ < 0.5 vol%. The samples underwent thermal post-processing in a furnace at 900 °C for 3 h using a heating ramp of 5 °C/min and allowing the furnace to naturally cool down to enable crack healing. The goodness of the parameter set was assessed by measuring the Archimedean density of the cubes in acetone, accounting for the open porosity by measuring the weight of the infiltrated sample in a closed container to limit errors owing to acetone evaporation. This measurement technique is essentially described by the ASTM standard for the measurement of refractory bricks [2]; the difference is in the fluid employed. Density measurements were performed before and after healing. The theoretical density of the cubes before calcination was assumed to be the weighted average between the two powder constituents (4.06 g/cm³). Density of the cubes after calcination was corrected for each cube, assuming that the difference in weight occurring after the healing process was owing to the oxidation reaction of TiC into TiO₂ that can be expressed as



Provided the ratio of the molar mass of $\text{TiC}/\text{TiO}_2 = 0.749$ and assuming that the mass of alumina is constant before and after calcination, the mass of TiO₂ was estimated as follows:

$$\begin{aligned} \Delta m &= -(m_{\text{TiC},1} - m_{\text{TiC},2}) + m_{\text{TiO}_2} = -0.749 m_{\text{TiO}_2} + m_{\text{TiO}_2}, \quad m_{\text{TiO}_2} \\ &\approx 4 \cdot \Delta m, \end{aligned} \quad (2)$$

where m is the mass of the respective phase, and subscripts 1 and 2 represent the state before and after calcination, respectively. The estimated mass of TiO₂ was subsequently used to calculate the theoretical density of the healed sample.

Table 2 lists the processing parameters that lead to the highest densification. The layer thickness was set to 40 μm , for which the effective powder layer thickness could reach 150 μm and higher, as demonstrated in some existing studies [15,24]. In this study, different characterization techniques were employed on several samples, and their geometries were optimized for a particular analytical method, which is summarized in Table 3. The PBF-manufactured samples before thermal treatment are referred as “As-prepared.” The parts that underwent thermal post-processing are named “Healed”

The cross-sections of 12 samples (from CP1 to CH3 in Table 3) were prepared by polishing using different diamond suspensions (from 9 to 1 μm). One half of the samples (from CP1 to CH3) were coated with a 5-nm layer of Pt/Pd and analyzed using SEM (JEOL, JSM7100F) equipped with an energy-dispersive X-ray spectroscopy (EDX) detector (Ametek-EDAX EDX) for elemental analysis. The phase composition of the remaining half (CP1 to CH3) was analyzed using the X-ray powder diffraction performed in Bragg-Brentano geometry using an AXS D8 ADVANCE (BRUKER) diffractometer equipped with a Cu-K α X-ray source. The data were acquired in a 2θ range from 5 to 120° with steps of 0.02° and an exposure time of 1 s per step. The mechanical characterization was performed using a biaxial flexural test, ball on three balls (B3Bs), using

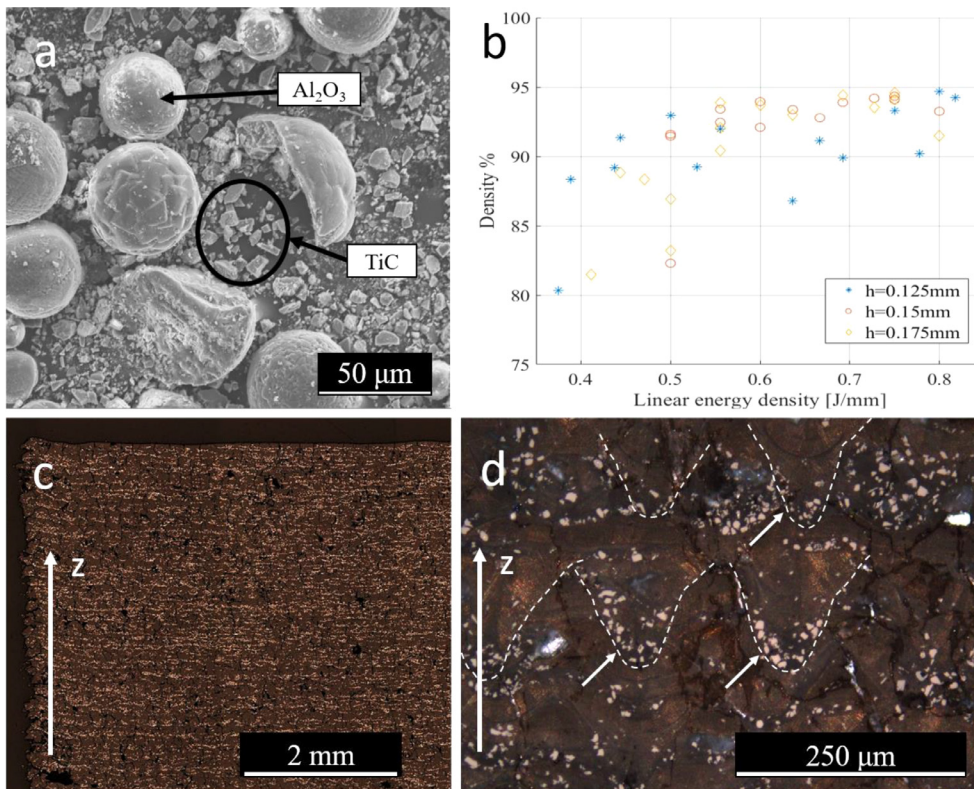


Fig. 1. (a) SEM picture of the powder mixture. The large spherical particles are alumina granules, whereas the fragmented powder are TiC particles. (b) Densification of the parts [%] for different hatch distances as a function of the laser linear energy density. (c) Upper quarter of a cube CP2 cross-section. (d) Higher magnification of the same sample showing clusters of TiC at the bottom of the melt pool, parameter-set 3 from Table 2.

Table 2
Parameter-sets leading to the highest part density.

ID	Laser power [W]	Scanning Speed [mm/s]	Hatch distance [mm]	Layer thickness [μm]
1	60	80	0.150	40
2	90	120	0.175	40
3	90	130	0.175	40

Table 3
Samples identification.

Sample ID	Building parameter Table 2	Status	Geometry	Dimensions mm	Number of samples
CP1	1	As-prepared	cube cut in half	5 × 10 × 10	2
CP2	2	As-prepared	cube cut in half	5 × 10 × 10	2
CP3	3	As-prepared	cube cut in half	5 × 10 × 10	2
CH1	1	Healed	cube cut in half	5 × 10 × 10	2
CH2	2	Healed	cube cut in half	5 × 10 × 10	2
CH3	3	Healed	cube cut in half	5 × 10 × 10	2
CY	1	Healed	cylinder	Ø 5.5 × 6	3
D	1	Healed	disk cut from CY	Ø 5.5 × 0.7	9

Zwick Roell Z005 on sample D made by slicing the cylinders CY, as presented in Table 3.

The first 2 mm of the CY sample and the upper part were discarded to avoid the influence of the substrate and the roughness of the upper layer. Three disks were obtained from each cylinder (sample D). Disk D was tested “as-cut,” implying that no further surface polishing was performed. The maximal stress at breakage was calculated as described by Börger et al. [5] assuming a Poisson’s ratio of $\nu = 0.25$.

3. Results and discussions

3.1. Laser processing

The density of highly performant ceramics is its primary characteristic. The density of the As-prepared sample as a function of the laser linear energy density P/v , defined as the ratio between the laser power

and scanning velocity, is shown in Fig. 1(b). For all the applied hatch distances (0.150, 0.175, and 0.125 mm), the densification limit was reached at approximately 94% of the calculated theoretical density. A hatch distance of 0.125 mm leads to more scattered and unpredictable results, which in some cases result in parts that would fall apart during removal from the substrate. The hatch distances of 0.150 and 0.175 mm exhibit comparable trends with respect to densification. The processing window (range of laser parameters resulting in solidified parts) for these hatch values appeared to be relatively broad. An increase in the linear energy density is typically associated with a higher part density. According to Fan et al. [9], the melt pool temperature of alumina can reach 3500 °C, which exceeds the melting temperature of TiC (3160 °C). Therefore, it is important to assess the presence of TiC within the Al_2O_3 matrix and to avoid the formation of unwanted intermediate compounds that might remain stable at high temperatures, thereby hindering the healing process by TiC oxidation. In addition, the dispersion of TiC within the

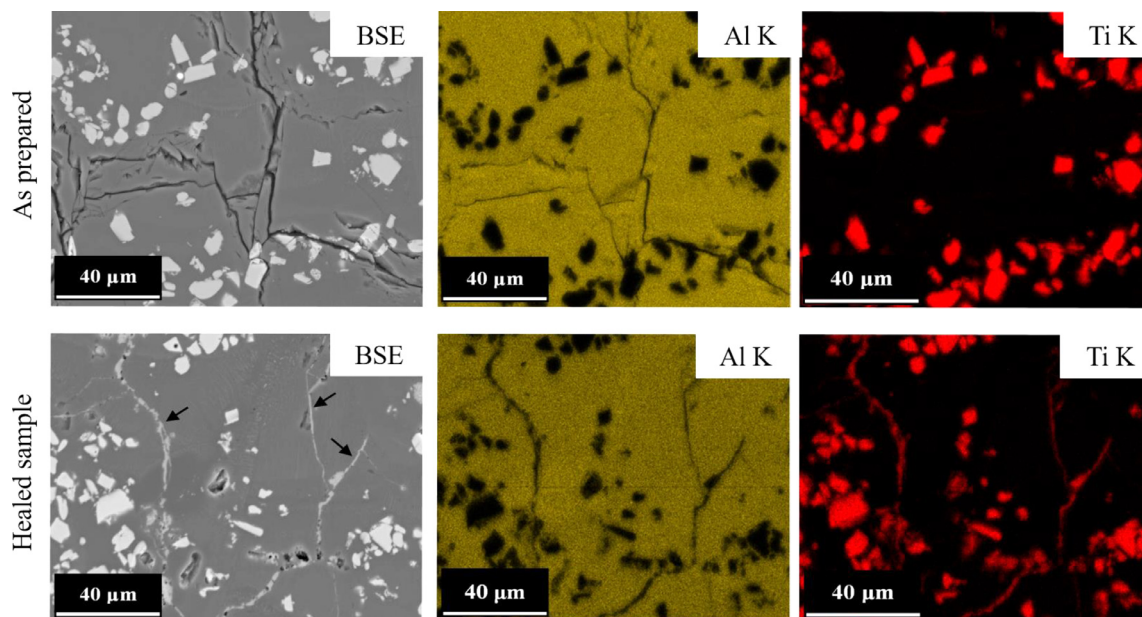


Fig. 2. SEM and EDX of samples before and after healing of the center of a 10 mm × 10 mm × 10 mm cube. The upper row shows the microstructure of an as-printed sample (CP3). The Ti distribution map shows no presence of Ti within the cracks. The bottom row shows the microstructure of the healed sample (CH3). In this case, the corresponding EDX map shows the presence of Ti inside the cracks.

alumina matrix is a significant aspect to verify. Fig. 1(c) illustrates the upper quadrant of the cube CP2 cross-section under a polarized light. The TiC (the light gray) particles agglomerate along lines perpendicular to the building direction. Fig. 1(d) shows a higher magnification image of the same cube, revealing that the TiC particles are mainly clustered at the bottom of the melt pool. The TiC particles exhibit a similar size and shape, as shown in Fig. 1(a); therefore, it indicates that high temperature of the liquid alumina bath does not affect TiC.

3.2. Crack healing

The main objective of this study was to assess the healing capability of the Al_2O_3 -TiC composite produced by PBF-LB. The healing was qualitatively assessed through the analysis of the crack-filling made by SEM and EDX at the surface and in the center of the samples. No significant differences were observed between these regions considering crack-filling behavior. The upper row in Fig. 2 represents the inner part of CP3 (As-prepared). Cracks are clearly visible within the alumina matrix indicated by the dark gray color along with the TiC particles represented by the light gray color. The EDX maps allow for a clear distinction between the alumina matrix and TiC particles. The bottom row of Fig. 2 shows the inner region of CH3. A third phase, identified as rutile by XRD, is present within the cracks. In Fig. 3, the phase filling the cracks and the sites where the TiC particles initiated healing, are marked with a star. The residual porosity in the region where TiC is present, is clearly visible. This porosity may be caused by an excess of CO_x gas production during TiC oxidation or simply by an insufficient availability of healing agent close to the defect, resulting in a partial healing. Additionally, the characteristic shape of the TiC particles is lost, adopting a more rounded shape according to the available space. A sub-micrometer pattern of TiC surrounded by alumina is highlighted within the circles in Fig. 3. It was hypothesized that this structure was formed during the melting of TiC. This pattern was visible in both the Healed and As-prepared samples.

The XRD measurements proved that the use of three different sets of parameters, as listed in Table 2, did not result in any clear differences in the diffraction data. Fig. 4 presents the powder diffraction patterns measured for the As-prepared sample (the upper pattern) and a Healed sample (the lower pattern). The data analysis revealed that right after

the laser processing, the samples are composed of corundum phase and TiC with rock salt structure with a minor contribution of TiO , also having a rock salt structure. The Healed samples, in addition to Al_2O_3 , TiC, and TiO , contain a significant amount of TiO_2 phase in the form of rutile.

The average mass of samples after healing exhibits a systematic increase ($\bar{X} = 0.27 \text{ g}$; $S_x = 0.026 \text{ g}$), which is consistent with the mass gain related to the transition from TiC to rutile. In addition, the average density slightly increased ($\bar{X} = 0.92\%$; $S_x = 0.46\%$), with a maximum and minimum density increase of 1.85 and 0.03%, respectively. The mechanical test was conducted using a B3Bs testing rig, as described by Danzer et al. [7]. It was important to investigate disks (sample D) extracted from larger cylinders (samples CY), after which the latter was healed. This provides a representative measure of the healing capabilities of a significant volume and far from the upper and lower surfaces of the samples. The mechanical properties of the As-prepared samples were not assessed because the disks had already broken during gentle wire cutting. Disks D cut from cylinder CY recorded an average ultimate strength of $181 \pm 27 \text{ MPa}$, calculated for nine samples, with minimal and maximal values of 139.7 and 232.7 MPa, respectively. Fig. 5(b) shows a back-scatter electron microscopy image of a disk surface after cutting. It is possible to discern the scanning pattern orthogonal to each other, rising defects as a lack of densification of the sample. The production and healing of an entire cylinder proved that strength recovery is effective even for larger volumes.

The relationship between the powder rheological properties and densities of the parts has been thoroughly described for metals and polymers [33]. Wilkes et al. [36] highlighted this relationship for ceramics by processing spherical and irregularly shaped powders of alumina and zirconia mixture, indicating that the impaired rheological behavior caused by the addition of TiC particles has a negative effect on the densification of the parts. Thus, the production of highly flowable granules may positively affect the process, leading to improved mechanical properties.

Zheng et al. [39] studied the orientation of cracks produced by PBF-LB in the Al_2O_3 samples. They distinguished transverse and longitudinal crack categories linked to the scanning direction, implying that these defects can be tuned using laser scanning. TiO_2 filling these oriented cracks may potentially result in advantageous macroscopic mechanical properties, which will be investigated in our future study.

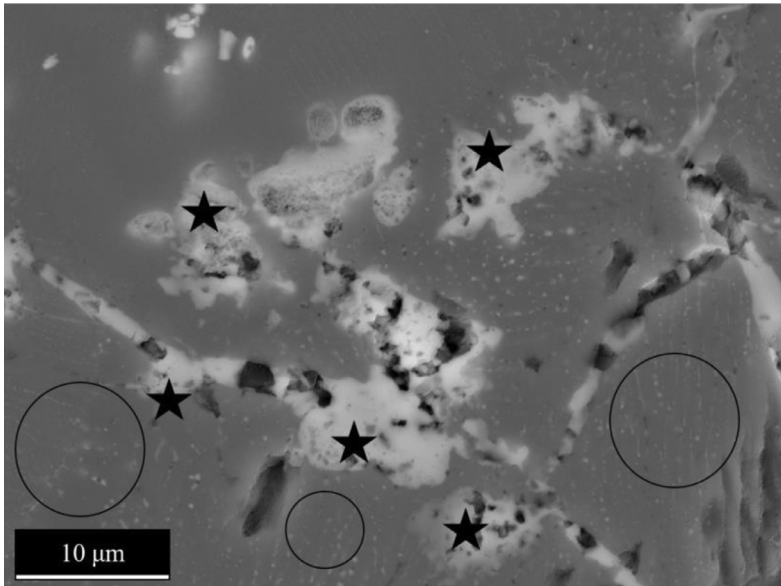


Fig. 3. Backscatter electrons composition SEM picture of the cross-section center of a cube. The cracks are partially filled. It shows a residual porosity and the position of the healing particle that contributed to the crack filling. An Al_2O_3 -TiC structure is evident within the circles.

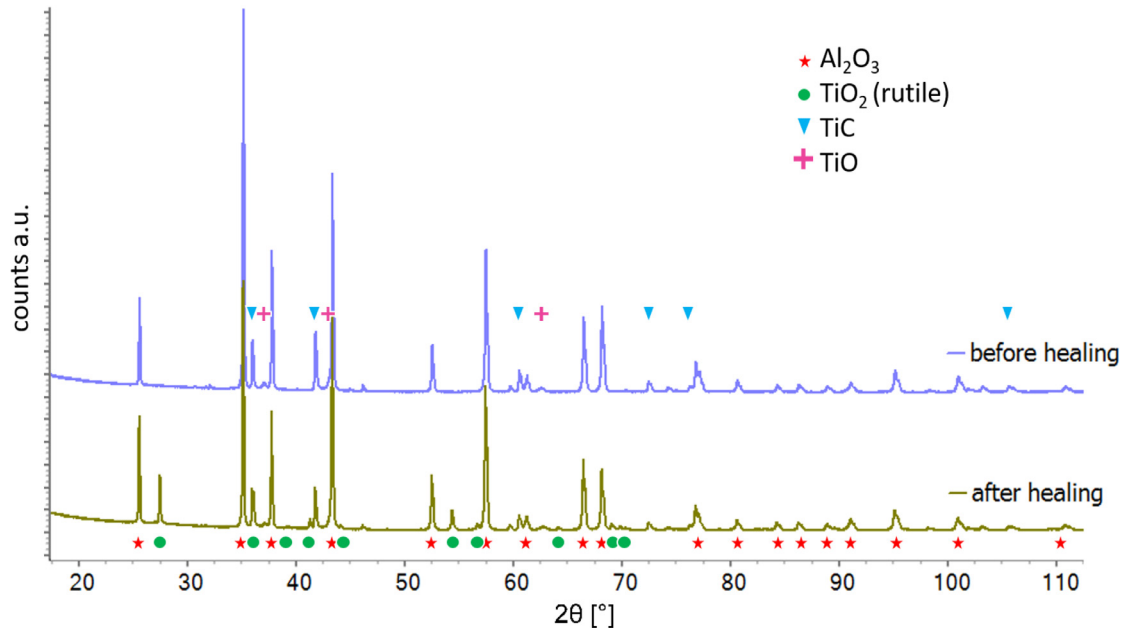


Fig. 4. Powder diffraction pattern for the As-prepared and Healed samples. The characteristic peak angles are highlighted with a symbol: star for Alumina, circle for Titanium dioxide, triangle for titanium carbide, and a cross for titanium monoxide.

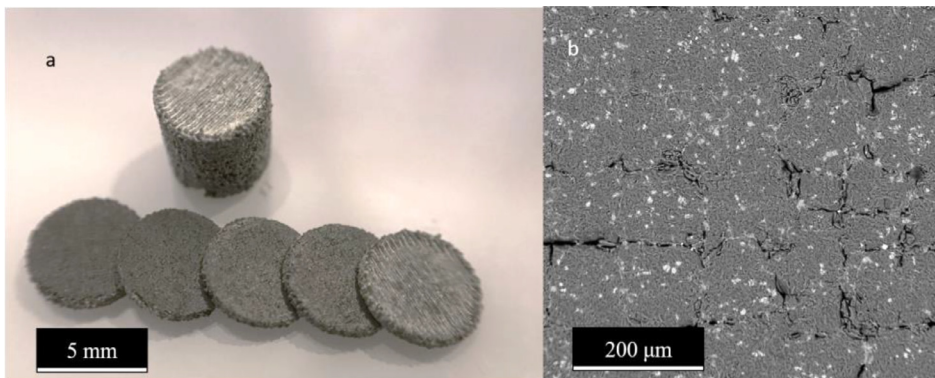


Fig. 5. (a) Entire healed cylinder and disks produced from it for the B3Bs test. (b) higher magnification (BSE) of the surface of one disk.

4. Conclusion

In this study, we introduced a viable alternative for the production of ceramic oxides using the PBF-LB technique. Parts with densities up to 94% were successfully produced by PBF using a conventional Nd:YAG laser. While a simple thermal post-processing exhibited a negligible effect on the mechanical properties of ceramic parts produced using PBF, whereas a significant improvement in flexural strength was achieved using the demonstrated healing process. The successful filling of cracks down to the core of the investigated parts was demonstrated for a ceramic material starting from a composite of alumina with the addition of 10 vol% TiC. This healing method can be employed to heal crack opening distances up to 2 μm and few hundred micrometers in length. Furthermore, the TiC particles did not melt within the alumina melt bath, and they were generally unaffected by the laser process. The segregation of TiC within the melt track may affect the healing capabilities, particularly on the upper surface of the samples, because TiC gathers at the bottom of the melt pool. The XRD measurements showed that the major phases present after the laser processing were the same as before the powder melting, namely alumina and TiC, agreeing with the SEM results. Therefore, TiC maintains its form and composition during the laser processing before being converted into TiO_2 during the healing process. The TiC particles in the proximity of cracks react to TiO_2 , whereas the TiC particles fully embedded in the alumina matrix do not contribute to the healing process. A flexural strength of 232 MPa was the highest recorded ultimate strength of an alumina matrix-based composite processed at room temperature using the PBF-LB technique.

Declaration of Competing Interest

The authors declare that they have no known competing financial interests or personal relationships that could have appeared to influence the work reported in this paper.

Acknowledgments

The authors would like to thank the Scientific center for Optical and Electron Microscopy (ScopeM, Zurich), Dr. L. Grafalha Morales for the microscopy training, and Prof. Dr. T. Graule (Empa) for providing access to the mechanical testing equipment.

References

- [1] K. Ando, B. Kim, M. Chu, S. Saito, K. Takahashi, Crack-healing and mechanical behavior of $\text{Al}_2\text{O}_3/\text{SiC}$ composites at elevated temperature, *Fatigue Fract. Eng. Mater. Struct.* 27 (1) (2004) 533–541.
- [2] ASTM C20-00, Standard test methods for apparent porosity, water absorption, apparent specific gravity, and bulk density of burned refractory brick and shapes by boiling water, *Am. Soc. Test. Mater.* (2015), doi:10.1520/C0020-00R10.2.
- [3] P. Bertrand, F. Bayle, C. Combe, P. Goeuriot, I. Smurov, Ceramic components manufacturing by selective laser sintering, *Appl. Surf. Sci.* 254 (4) (2007) 989–992, doi:10.1016/j.apsusc.2007.08.085.
- [4] L. Boatemaa, J.C. Brouwer, S. van der Zwaag, W.G. Sloof, The effect of the TiC particle size on the preferred oxidation temperature for self-healing of oxide ceramic matrix materials, *J. Mater. Sci.* 53 (8) (2018) 5973–5986, doi:10.1007/s10853-017-1973-x.
- [5] A. Börger, P. Supancic, R. Danzer, The ball on three balls test for strength testing of brittle discs: part II: analysis of possible errors in the strength determination, *J. Eur. Ceram. Soc.* 24 (10–11) (2004) 2917–2928, doi:10.1016/j.jeurceramsoc.2003.10.035.
- [6] D. Bourell, J.P. Kruth, M. Leu, G. Levy, D. Rosen, A.M. Beese, A. Clare, Materials for additive manufacturing, *CIRP Ann. Manuf. Technol.* 66 (2) (2017) 659–681, doi:10.1016/j.cirp.2017.05.009.
- [7] R. Danzer, W. Harrer, P. Supancic, T. Lube, Z. Wang, A. Börger, The ball on three balls test-strength and failure analysis of different materials, *J. Eur. Ceram. Soc.* 27 (2–3) (2007) 1481–1485, doi:10.1016/j.jeurceramsoc.2006.05.034.
- [8] H. Exner, P. Refenfuß, R. Ebert, Lasermikrosintern von keramischen Materialien, *RTE J.* 3 (3) (2006) 1–18 Retrieved from https://www.rtejournal.de/ausgabe3/347/Exner_Lasermikrosintern_von_keramischen_Materialien.pdf.
- [9] Z. Fan, M. Lu, H. Huang, Selective laser melting of alumina: a single track study, *Ceram. Int.* 44 (8) (2018) 9484–9493, doi:10.1016/j.ceramint.2018.02.166.
- [10] L. Ferrage, G. Bertrand, P. Lenormand, Dense yttria-stabilized zirconia obtained by direct selective laser sintering, *Addit. Manuf.* 21 (April) (2018) 472–478, doi:10.1016/j.addma.2018.02.005.
- [11] K. Florio, S. Pfeiffer, M. Makowska, N. Casati, F. Verga, H. Moens-Van Swyghoven, K. Wegener, T. Graule, An innovative selective laser melting process for hematite-doped aluminum oxide, *Adv. Eng. Mater.* (2019) 1–10 tbp, doi:10.1002/adem.201801352.
- [12] A. Gahler, J.G. Heinrich, J. Günster, Direct laser sintering of $\text{Al}_2\text{O}_3\text{-SiO}_2$ dental ceramic components by layer-wise slurry deposition, *J. Am. Ceram. Soc.* (2006), doi:10.1111/j.1551-2916.2006.01217.x.
- [13] M.X. Gan, C.H. Wong, Experimental studies on the properties of selectively laser melted alumina-spodumene composite, *Ceram. Int.* 44 (15) (2018) 19008–19015, doi:10.1016/j.ceramint.2018.07.144.
- [14] P. Greil, Generic principles of crack-healing ceramics, *J. Adv. Ceram.* (2012), doi:10.1007/s40145-012-0020-2.
- [15] L. Haferkamp, A. Spierings, M. Rusch, D. Jermann, M.A. Spurek, K. Wegener, Effect of particle size of monomodal 316 L powder on powder layer density in powder bed fusion, *Prog. Addit. Manuf.* (2020) 0123456789, doi:10.1007/s40964-020-00152-4.
- [16] Hagedorn, Y. (2013). Additive manufacturing of high performance oxide ceramics via selective laser melting (Issue August) [RWTH Aachen]. Retrieved from <http://publications.rwth-aachen.de/record/229055>
- [17] Y. Hagedorn, J.I. Wilkes, W. Meiners, K. Wissenbach, R. Poprawe, Net shaped high performance oxide ceramic parts by selective laser melting, *Phys. Procedia* 5 (Part 2) (2010) 587–594, doi:10.1016/j.phpro.2010.08.086.
- [18] J.G. Heinrich, A. Gahler, J. Günster, M. Schmücker, J. Zhang, D. Jiang, M. Ruan, Microstructural evolution during direct laser sintering in the $\text{Al}_2\text{O}_3\text{-SiO}_2$ system, *J. Mater. Sci.* 42 (14) (2007) 5307–5311, doi:10.1007/s10853-006-1247-5.
- [19] E. Juste, F. Petit, V. Lardot, F. Cambier, Shaping of ceramic parts by selective laser melting of powder bed, *J. Mater. Res.* 29 (17) (2014) 2086–2094, doi:10.1557/jmr.2014.127.
- [20] G. Kaur, V. Kumar, F. Bains, J.C. Mauro, G. Pickrell, I. Evans, O. Bretcanu, Mechanical properties of bioactive glasses, ceramics, glass-ceramics and composites: state-of-the-art review and future challenges, *Mater. Sci. Eng. C* 104 (2019) 109895 December 2018, doi:10.1016/j.msec.2019.109895.
- [21] R.S. Khmyrov, C.E. Protasov, S.N. Grigoriev, A.V. Gusarov, Crack-free selective laser melting of silica glass: single beads and monolayers on the substrate of the same material, *Int. J. Adv. Manuf. Technol.* 85 (5–8) (2016) 1461–1469, doi:10.1007/s00170-015-8051-9.
- [22] H.E. Kim, A.J. Moorhead, Oxidation behavior and effects of oxidation on the strength of SiC-whisker reinforced alumina, *J. Mater. Sci.* 29 (6) (1994) 1656–1661, doi:10.1007/BF00368941.
- [23] I.S. Lee, Rapid full densification of alumina-glass composites fabricated by a selective laser sintering process, *J. Mater. Sci. Lett.* 17 (22) (1998) 1907–1911, doi:10.1023/A:1006600208059.
- [24] Y. Mahmoodkhani, U. Ali, S. Imani Shahabad, A. Rani Kasinathan, R. Esmaeilzadeh, A. Keshavarzkermani, E. Marzbanrad, E. Toyserkani, On the measurement of effective powder layer thickness in laser powder-bed fusion additive manufacturing of metals, *Prog. in Addit. Manuf.* 4 (2) (2019) 109–116, doi:10.1007/s40964-018-0064-0.
- [25] L. Moniz, C. Colin, J.D. Bartout, K. Terki, M.H. Berger, Laser beam melting of alumina: effect of absorber additions, *JOM* (2018), doi:10.1007/s11837-017-2716-9.
- [26] T. Osada, T. Hara, M. Mitome, S. Ozaki, T. Abe, K. Kamoda, T. Ohmura, Self-healing by design: universal kinetic model of strength recovery in self-healing ceramics, *Sci. Technol. Adv. Mater.* 21 (1) (2020) 593–608, doi:10.1080/14686996.2020.1796468.
- [27] S. Pfeiffer, M. Makowska, Kevin Florio, D.F. Sanchez, F. Marone, X. Zhang, C.G. Anzeris, H. Van Swyghoven, K. Wegener, T. Graule, Selective laser melting of thermal pre-treated metal oxide doped aluminum oxide granules, *Open Ceram.* 100007 (2020) (2020) 100007, doi:10.1016/j.oceram.2020.100007.
- [28] P. Regenfuss, A. Streek, L. Hartwig, S. Klötzer, T. Brabant, M. Horn, R. Ebert, H. Exner, Principles of laser micro sintering, *Rapid Prototyp. J.* 13 (4) (2007) 204–212, doi:10.1108/13552540710776151.
- [29] P. Regenfuss, A. Streek, F. Ullmann, C. Kühn, L. Hartwig, M. Horn, R. Ebert, H. Exner, Laser micro sintering of ceramic materials, part 1, *Intereram* 57 (2008) 6–9.
- [30] Peter Regenfuss, A. Streek, L. Hartwig, S. Klötzer, T. Brabant, M. Horn, R. Ebert, H. Exner, Rapid prototyping journal principles of laser micro sintering, *Rapid Prototyp. J.* 13 (4) (2007) Rapid Prototyping Journal Iss Assembly Automation Retrieved from <https://doi.org/10.1108/13552540510573365%22%3Ehttps://doi.org/10.1108/13552540510573365%3C/a%3E>, doi:10.1108/13552540710776151.
- [31] I. Shishkovsky, I. Yadroitsev, P. Bertrand, I. Smurov, Alumina-zirconium ceramics synthesis by selective laser sintering/melting, *Appl. Surf. Sci.* 254 (4) (2007) 966–970, doi:10.1016/j.apsusc.2007.09.001.
- [32] R. Sugiyama, K. Yamane, W. Nakao, K. Takahashi, K. Ando, Effect of difference in crack-healing ability on fatigue behavior of alumina/silicon carbide composites, *J. Intell. Mater. Syst. Struct.* 19 (3) (2008) 411–415, doi:10.1177/1045389x07084943.
- [33] A.T. Sutton, C.S. Kriewall, M.C. Leu, J.W. Newkirk, Powder characterization techniques and effects of powder characteristics on part properties in powder-bed fusion processes, *Virtual Phys. Prototyp.* 12 (1) (2017) 3–29, doi:10.1080/17452759.2016.1250605.
- [34] F. Verga, M. Borlaf, L. Conti, K. Florio, M. Vetterli, T. Graule, M. Schmid, K. Wegener, Laser-based powder bed fusion of alumina toughened zirconia, *Addit. Manuf.* (31) (2020) 100959 June 2019, doi:10.1016/j.addma.2019.100959.
- [35] Wilkes, J.I. (2009). Selektives Laserschmelzen zur generativen herstellung von bauteilen aus hochfester oxidkeramik [RWTH Aachen]. Retrieved from <http://publications.rwth-aachen.de/record/51362>
- [36] J.I. Wilkes, Y. Hagedorn, W. Meiners, K. Wissenbach, Additive manufacturing of $\text{ZrO}_2\text{-Al}_2\text{O}_3$ ceramic components by selective laser melting, *Rapid Prototyp. J.* 19 (1) (2013) 51–57, doi:10.1108/13552541311292736.

- [37] D. Wu, F. Lu, D. Zhao, G. Ma, C. Li, J. Ding, F. Niu, Effect of doping SiC particles on cracks and pores of Al_2O_3 - ZrO_2 eutectic ceramics fabricated by directed laser deposition, *J. Mater. Sci.* (2019) 9321–9330, doi:[10.1007/s10853-019-03555-z](https://doi.org/10.1007/s10853-019-03555-z).
- [38] S. Yoshioka, L. Boatmaa, S. Zwaag, W. van der, Nakao, W.G. Sloof, On the use of TiC as high-temperature healing particles in alumina based composites, *J. Eur. Ceram. Soc.* 36 (16) (2016) 4155–4162, doi:[10.1016/j.jeurceramsoc.2016.06.008](https://doi.org/10.1016/j.jeurceramsoc.2016.06.008).
- [39] Y. Zheng, K. Zhang, T.T. Liu, W.H. Liao, C.D. Zhang, H. Shao, Cracks of alumina ceramics by selective laser melting, *Ceram. Int.* 45 (1) (2019) 175–184.
- [40] S. van der Zwaag, Self-Healing Materials: an Alternative Approach to 20 Centuries of Materials Science 100 (2007), doi:[10.1515/ci.2008.30.6.20](https://doi.org/10.1515/ci.2008.30.6.20).